SUPPLEMENTAL MATERIAL

Boldin et al., http://www.jem.org/cgi/content/full/jem.20101823/DC1

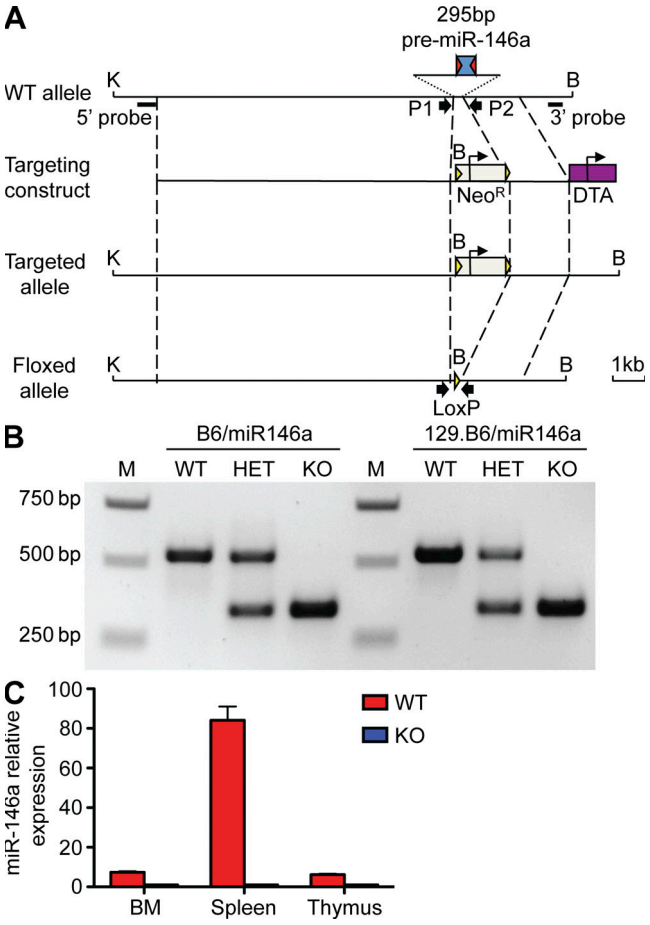

Figure S1. The generation of *miR-146a*–null mice. This figure is related to Fig. 1. (A) Schematic representation of *miR-146a* KO targeting strategy. To ablate miR-146a expression, we replaced a 295-bp fragment, containing all of miR-146a mouse precursor sequence, with a Neomycin resistance (Neo^R) cassette flanked by loxP sites by homologous recombination in embryonic stem cells. The Neo^R cassette was then floxed out by mating F1 generation heterozygous (*miR-146a*$^{+/Neo^R}$) mice with germline-expressing Cre recombinase transgenic animals (EIIa-Cre), resulting in a swap of miR-146a precursor sequence for a single loxP site. The locations of the 3′ and 5′ end Southern probes and PCR primers (P1 and P2) are depicted in the graph. B, BamHI; DTA, diphtheria toxin; K, KpnI. (B) Genomic PCR analysis confirming deletion of *miR-146a* locus. PCR was performed on genomic DNA from WT, *miR-146a*$^{+/-}$ (HET), and *miR-146a*$^{-/-}$ (KO) mice of two different genetic backgrounds (129.B6 mixed and pure C57BL/6), as indicated. M, molecular weight marker. (C) qRT-PCR analysis of mature miR-146a expression in hematopoietic tissues of WT and *miR-146a*$^{-/-}$ mice normalized by 5S rRNA levels. Quantitative PCR signal generated by *miR-146a*$^{-/-}$ sample for each tissue was arbitrarily set to 1. Data are represented as mean ± SD. The experiment in C was carried with the 129.B6/*miR-146a*$^{-/-}$ strain of mice. All other experiments were carried with B6/*miR-146a*$^{-/-}$ animals.

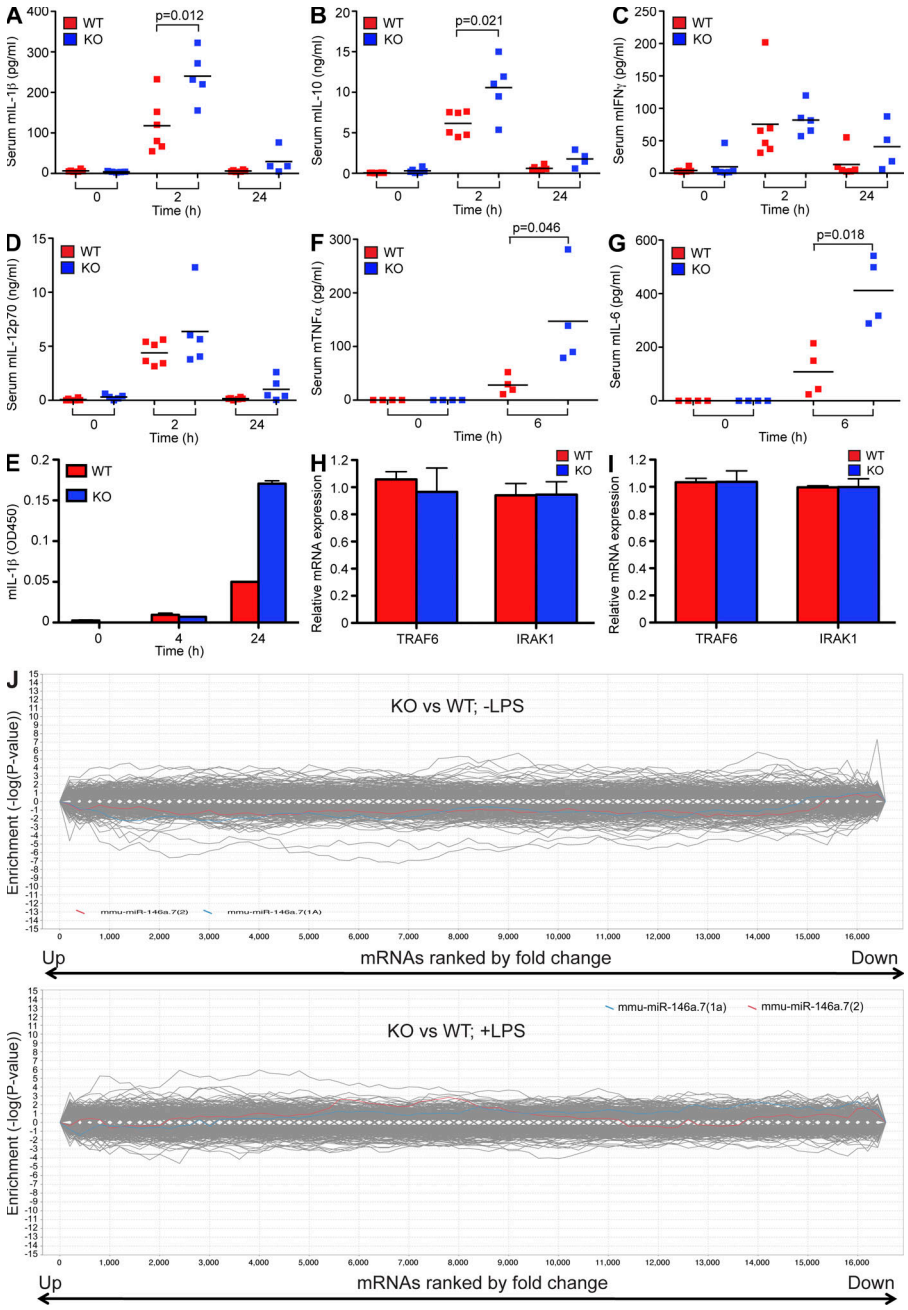

Figure S2. ELISA analyses of cytokine expression in serum of LPS-stimulated *miR-146a*–null mice and qRT-PCR and Sylamer analysis of gene expression in *miR-146a*–null BMDMs. This figure is related to Fig. 2. (A–D) ELISA analysis of IL-1β (A), IL-10 (B), IFN-γ (C), and IL-12 (D) levels in serum of *miR-146a*$^{-/-}$ (KO) and WT animals after sublethal 1 mg/kg LPS challenge. Peripheral blood was drawn at the time points indicated in the graph. Results are shown as means; data are representative of two independent experiments. (E) ELISA analysis of IL-1β secretion by *miR-146a*$^{-/-}$ (KO) and WT BMDMs in vitro after 10 ng/ml LPS stimulation. Cells were stimulated for the times indicated in the graph. Results are representative of three independent experiments. (F and G) Serum levels of TNF (F) and IL-6 (G) in *miR-146a*$^{-/-}$ (KO; $n = 4$) and WT ($n = 4$) animals challenged intraperitoneally with a lethal dose of LPS (35 mg/kg). Peripheral blood was drawn at the times indicated in the graphs, and cytokine concentrations were assessed by ELISA. (A–D, F, and G) P-value calculations were performed using Student's *t* test. (H and I) qRT-PCR analysis of TRAF6 and IRAK1 mRNA expression in BMDMs (H) and B cells (I) from WT and *miR-146a*$^{-/-}$ (KO) mice. Data are representative of two independent experiments. (E, H, and I) Data are shown as mean ± SD. (J) Analysis of global miR-146a target derepression in *miR-146a*–null BMDM cells. Microarray analysis showing enrichment and depletion of words corresponding to miRNA seed-matched heptamers in 3′ UTRs of transcripts using the Sylamer algorithm (van Dongen et al., 2008). The x axis represents the sorted gene list from most up-regulated in the *miR-146a* KO (left) to most down-regulated (right). The y axis shows the hypergeometric significance for enrichment or depletion of heptamers in 3′ UTRs at leading parts of the gene list. Positive values indicate enrichment (−log10(P value)), and negative values indicate depletion (log10(P value)). Expression profiles from cells that were treated with 10 ng/ml LPS for 24 h (bottom) or left untreated (top) were used for Sylamer analysis. Note that plots for two miR-146a heptamers matching the 5′ seed region, starting at positions 1 (blue line) and 2 (red line) show no significant enrichment, suggesting lack of global derepression of miR-146a target genes. The experiment in E was carried with the 129.B6/*miR-146a*$^{-/-}$ strain of mice. All other experiments were carried with B6/*miR-146a*$^{-/-}$ animals.

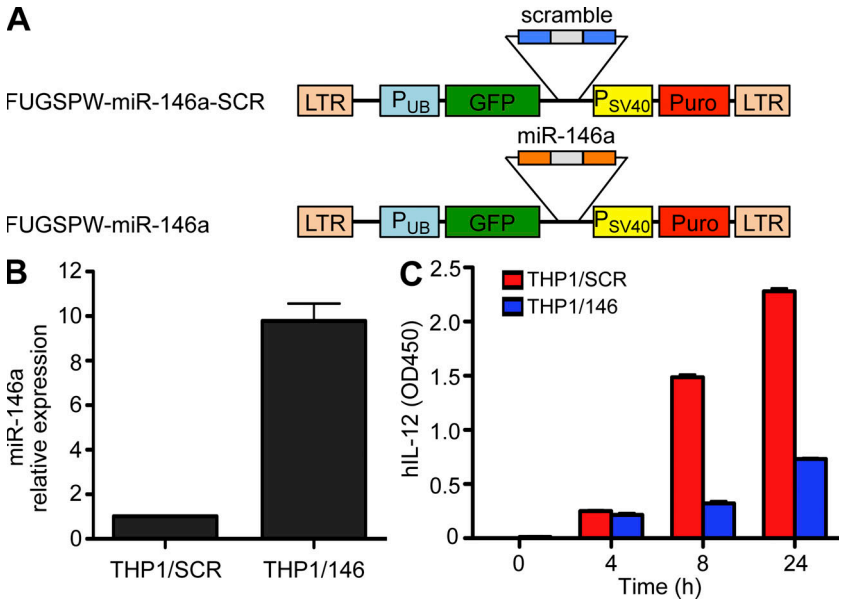

Figure S3. The generation of THP1/146 and THP1/SCR cells and analysis of IL-12 secretion in these cells in response to LPS. This figure is related to Fig. 3. (A) Schematic diagrams of lentiviral constructs used to generate stable THP-1 cell line overexpressing miR-146a. P_{UB}, ubiquitin promoter; P_{SV40}, immediate-early promoter from SV40 virus; Puro, puromycin-resistant gene. (B) qRT-PCR analysis of mature miR-146a expression in THP1/SCR and THP1/146 stable cell lines. Expression level of miR-146a in THP1/SCR was set to 1. (C) ELISA analysis of IL-12 secretion by THP1/SCR and THP1/146 cell lines. Cells were stimulated with 1 µg/ml LPS for the times indicated in the graph. Data are representative of two independent experiments. (B and C) Data are represented as mean ± SD. Experiments were carried with B6/*miR-146a*$^{-/-}$ animals.

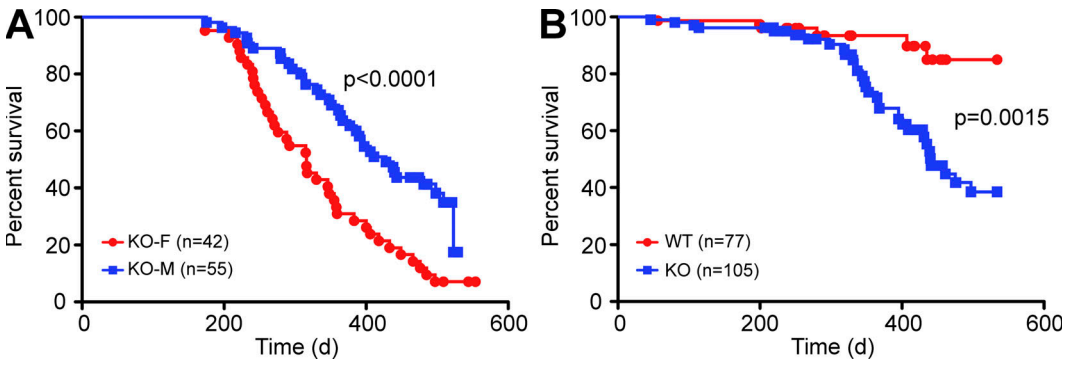

Figure S4. Kaplan-Meier survival curves for males and females from the 129.B6/*miR-146a*$^{-/-}$ line and lifespan for the B6/*miR-146a*$^{-/-}$ line. This figure is related to Fig. 4. (A) Kaplan-Meier survival curves of male (KO-M) and female (KO-F) *miR-146a*–null animals on 129.B6 background. (B) Kaplan-Meier survival curves of WT and *miR-146a*$^{-/-}$ (KO) mouse populations on C57BL/6 background. (A and B) P-value calculations were performed using log-rank (Mantel-Cox) test. The experiment in A was carried with the 129.B6/*miR-146a*$^{-/-}$ strain of mice. The experiment in B was carried with B6/*miR-146a*$^{-/-}$ animals.

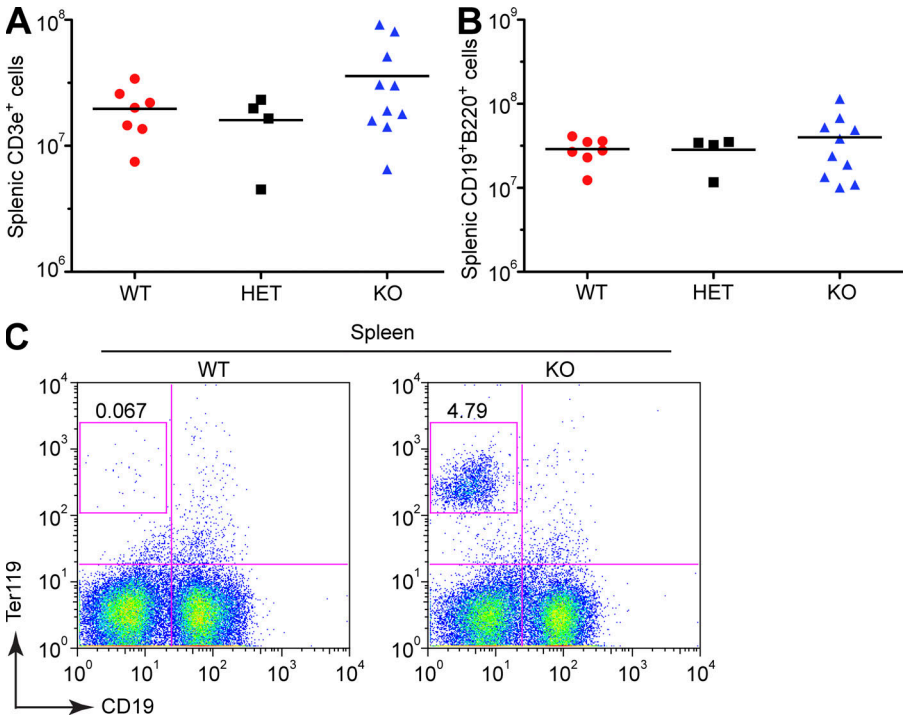

Figure S5. Absolute T and B cells counts and extramedullary hematopoiesis in *miR-146a*–null spleens. This figure is related to Fig. 5. (A and B) Absolute counts of T cells ($CD3^+$; A) and B cells ($CD19^+B220^+$; B) in WT ($n = 7$), *miR-146a*$^{+/-}$ (HET; $n = 4$), and *miR-146a*$^{-/-}$ (KO; $n = 10$) spleens. Results are shown as means and are representative of two independent experiments. The differences between groups were not statistically significant; p-value calculations were performed using Student's *t* test. (C) Extramedullary hematopoiesis in *miR-146a*–null animals. FACS analysis of splenocytes for erythroid ($Ter119^+$) and B cell ($CD19^+$) populations in WT and KO animals. Numbers indicate percentage of cells in the gate. Results are representative for at least three independent experiments. The experiments in A and B were carried with the 129.B6/*miR-146a*$^{-/-}$ strain of mice. The experiment in C was carried with B6/*miR-146a*$^{-/-}$ animals.

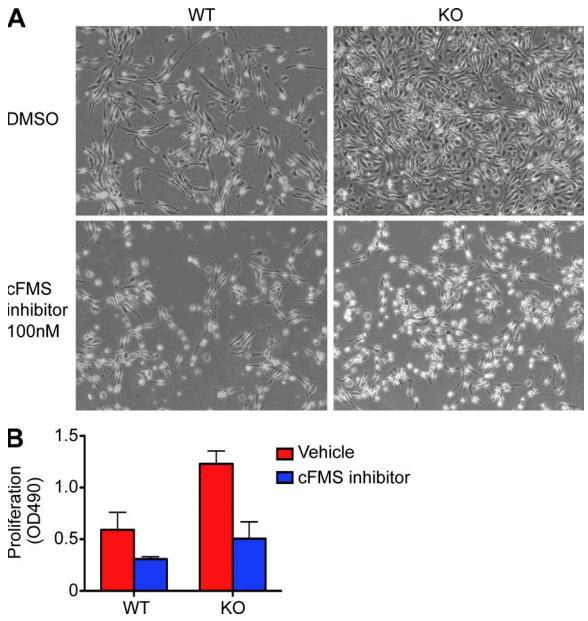

Figure S6. Pharmacological inhibition of CSF1R activity blocks BMDM proliferation. This figure is related to Fig. 6. (A) Photographs of proliferating in response to 50 ng/ml M-CSF BMDM cultures from WT and *miR-146a*$^{-/-}$ (KO) mice. Cells were treated with either 100 nM CSF1R inhibitor (bottom) or vehicle (top). Pictures were taken on day 4 after cell plating and are representative of several biological replicates. Note more robust proliferation of cells in the *miR-146a*–null BMDM culture and its block by addition of CSF1R inhibitor (EMD). (B) Quantification of cellular proliferation of differentiating BMDM cultures from WT and *miR-146a*$^{-/-}$ mice in the presence (blue) or absence (red) of CSF1R inhibitor. BMDM differentiation was stimulated with 50 ng/ml M-CSF. Cell proliferation was assessed by MTS assay on day 4 after cell plating. Data are represented as mean ± SD. Experiments were carried with B6/*miR-146a*$^{-/-}$ animals.

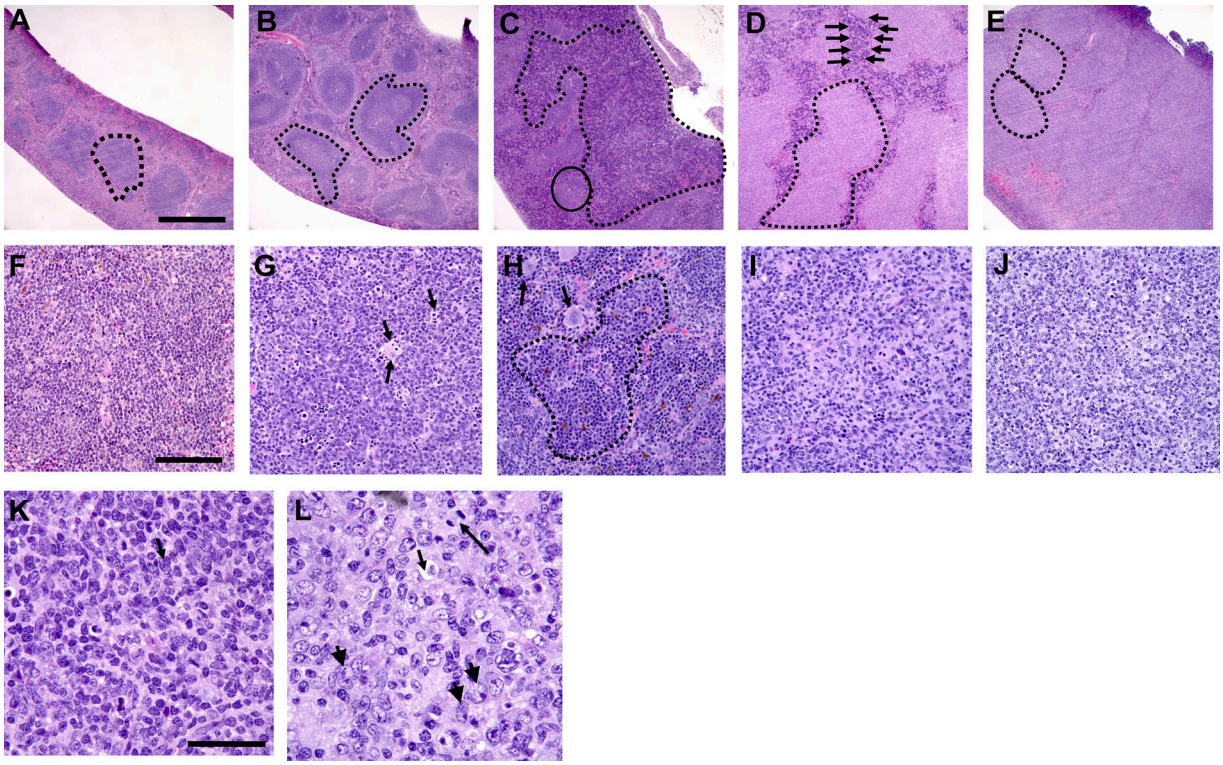

Figure S7. Characterization of tumorigenesis stages in *miR-146a*–null mice. This figure is related to Fig. 7. (A) Spleen from WT mouse. Note small follicles (one follicle is outlined by a dotted line) with extensive spacing between lymphoid areas (preserved red pulp). (B) Follicular hyperplasia in *miR-146a* mutant mouse. Note that there are more follicles and they are larger than those seen in A. The follicles (outlined by dotted lines) have a light central region (germinal center) and a darker rim of lymphocytes (mantle zone), confirming preserved architecture seen in hyperplasia. (C) Extramedullary hematopoiesis and myeloid proliferation (outlined by the dotted line) in *miR-146a*–deficient mouse. An adjacent, compressed lymphoid follicle is outlined by a solid line. (D) Low-grade follicular lymphoma in *miR-146a* KO mouse. Note expanded follicles lacking mantle zones (outlined by a dotted line). Entrapped between these enlarged follicles are residual splenic hematopoietic elements (between the arrows). (E) High-grade follicular lymphoma in an *miR-146a* KO mouse. Note here follicles are back to back (outlined by dotted lines) with no intervening red pulp. (F) Medium-power image of WT spleen in A. Note that the WT follicles are composed of bland-looking small lymphocytes. (G) Medium-power image of follicular hyperplasia in *miR-146a* mutant mouse in B. Note that the follicles show increased mitoses and apoptotic bodies (in so-called tingible body macrophages; arrows). (H) Medium-power image of extramedullary hematopoiesis and myeloid proliferation in *miR-146a*–deficient mouse in C. The expansion of the red pulp in some *miR-146a* KO mice is accompanied by increased splenic hematopoiesis as demonstrated by the expansion of erythroid islands (dotted line) and increased numbers of megakaryocytes (arrows). (I) Medium-power image of low-grade follicular lymphoma in miR-146a KO mouse (D). (J) Medium-power image of high-grade follicular lymphoma in *miR-146a* KO mouse in E. (K) High-power appearance of low-grade follicular lymphoma shows medium-sized lymphocytes and rare mitotic figures. Scattered large cells are present (arrow). (L) High-power appearance of high-grade follicular lymphoma shows apoptotic figures (medium arrow), mitotic figures (long arrow), and numerous large cells (short arrows). All sections were stained with hematoxylin and eosin. See more explanation in section Aging miR-146a–null mice develop tumors. Bars: (A–E) 1 mm; (F–J) 100 µm; (K and L) 40 µm. Experiments were carried with the 129.B6/*miR-146a*$^{-/-}$ strain of mice.

Table S1, included as an Excel file, is a list of differentially expressed genes in untreated *miR-146a*$^{-/-}$ BMDMs.
Table S2, included as an Excel file, is a list of differentially expressed genes in LPS-treated *miR-146a*$^{-/-}$ BMDMs.

REFERENCE

van Dongen, S., C. Abreu-Goodger, and A.J. Enright. 2008. Detecting microRNA binding and siRNA off-target effects from expression data. *Nat. Methods.* 5:1023–1025. doi:10.1038/nmeth.1267